CHEMISTRY
A EUROPEAN JOURNAL

DOI: 10.1002/chem.200700467

Is This a Chemical Bond? A Theoretical Study of $Ng_2@C_{60}$ (Ng = He, Ne, Ar, Kr, Xe)

Andreas Krapp and Gernot Frenking*[a]

Dedicated to Professor Roald Hoffmann on the occasion of his 70th birthday

Abstract: Quantum-chemical calculations using DFT (BP86) and ab initio methods (MP2, SCS-MP2) have been carried out for the endohedral fullerenes $Ng_2@C_{60}$ (Ng = He–Xe). The nature of the interactions has been analyzed with charge- and energy-partitioning methods and with the topological analysis of the electron density (Atoms-in-Molecules (AIM)). The calculations predict that the equilibrium geometries of $Ng_2@C_{60}$ have D_{3d} symmetry when Ng = Ne, Ar, Kr, while the energy-minimum structure of $Xe_2@C_{60}$ has D_{5d} symmetry. The precession movement of He_2 in $He_2@C_{60}$ has practically no barrier. The Ng–Ng distances in $Ng_2@C_{60}$ are much shorter than in free Ng_2. All compounds $Ng_2@C_{60}$ are thermodynamically unstable towards loss of the noble gas atoms. The heavier species $Ar_2@C_{60}$, $Kr_2@C_{60}$, and $Xe_2@C_{60}$ are high energy compounds which are at the BSSE corrected SCS-MP2/TZVPP level in the range 96.7–305.5 kcal mol^{-1} less stable than free $C_{60} + 2\,Ng$. The AIM method reveals that there is always an Ng–Ng bond path in $Ng_2@C_{60}$. There are six Ng–C bond paths in (D_{3d}) $Ar_2@C_{60}$, $Kr_2@C_{60}$, and $Xe_2@C_{60}$, whereas the lighter D_{3d} homologues $He_2@C_{60}$ and $Ne_2@C_{60}$ have only three Ng–C_2 paths. The calculated charge distribution and the orbital analysis clearly show that the bonding situation in $Xe_2@C_{60}$ significantly differs from those of the lighter homologues. The atomic partial charge of the [Xe_2] moiety is +1.06, whereas the charges of the lighter dimers [Ng_2] are close to zero. The a_{2u} HOMO of (D_{3d}) $Xe_2@C_{60}$ in the $^1A_{1g}$ state shows a large mixing of the highest lying occupied σ* orbital of [Xe_2] and the orbitals of the C_{60} cage. There is only a small gap between the a_{2u} HOMO of $Xe_2@C_{60}$ and the e_u LUMO and the a_{2u} LUMO + 1. The calculations show that there are several triplet states which are close in energy to each other and to the $^1A_{1g}$ state. The bonding analysis suggests that the interacting species in $Xe_2@C_{60}$ are the charged species Xe_2^{q+} and C_{60}^{q-}, where $1 < q < 2$. The calculated Xe–Xe distance in the endohedral fullerene (2.494 Å) is even shorter than the calculated value for free Xe_2^{2+} (2.746 Å). Thus, the Xe–C and Xe–Xe interactions in $Xe_2@C_{60}$ should be considered as genuine chemical bonds which are enforced by the compression energy. The Ng–Ng and Ng–C interactions in the lighter homologues $Ar_2@C_{60}$ and $Kr_2@C_{60}$ may also be considered as chemical bonds because the theoretically predicted properties of the endohedral fullerenes are significantly different from the free C_{60} and noble gas atoms. According to the bonding analysis, $He_2@C_{60}$ and $Ne_2@C_{60}$ are weakly bonded van der Waals complexes.

Keywords: chemical bonding · density functional calculations · endohedral fullerenes · energy decomposition analysis

Introduction

According to the 1997 definition of IUPAC, "*there is a chemical bond between two atoms or groups of atoms in the case that the forces acting between them are such as to lead to the formation of an aggregation with sufficient stability to make it convenient for the chemist to consider it as an independent 'molecular species'*".[1] This definition, which was adopted from Pauling,[2] leaves some ambiguity concerning the nature of a molecular species, but most chemists will have no difficulty in distinguishing between a molecule and a weakly bonded aggregate such as a noble gas dimer Ng_2 which is held together by weak van der Waals forces. Straightforward application of quantum mechanical laws in terms of the Atoms-in-Molecules (AIM) theory provides an-

[a] Dipl.-Chem. A. Krapp, Prof. G. Frenking
Fachbereich Chemie, Philipps-Universität Marburg
Hans-Meerwein-Strasse, 35043 Marburg (Germany)
Fax: (+49) 6421-282-5566
E-mail: Frenking@chemie.uni-marburg.de

Supporting information for this article is available on the WWW under http://www.chemeurj.org or from the author.

other definition of a bond. According to Bader, two atoms are bonded to each other if there is a bond path, which is a line of maximum electron density in a system in stable electrostatic equilibrium, connecting the neighboring nuclei.[3] The two definitions may be considered as exemplary for the differences between chemistry and physics in their respective approaches to describing the material world. The existence of a bond path alone does not distinguish between a strong bond in a molecule and weak interatomic attractions such as in He_2. This recently led to controversial discussions about the usefulness of the bond path as an indicator of a chemical bond.[4–9] In particular, there is disagreement between adherents of the traditional bond model and bond path followers to define the nature of interatomic interactions when repulsive forces play a significant role in the interatomic interactions. Two examples that have been discussed recently in the literature (Scheme 1) will be elaborated, since they are relevant to the present work.

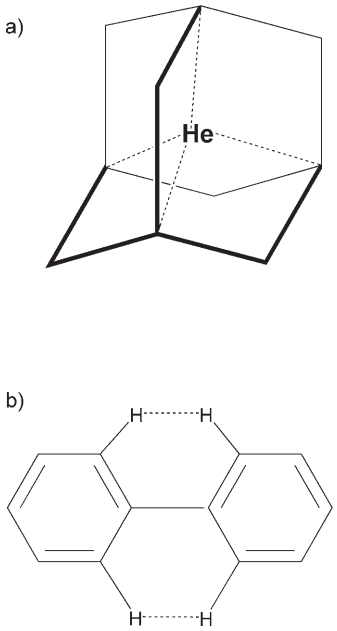

Scheme 1. Molecules with putative chemical bonds.

The first example concerns the nature of the hydrogen–hydrogen interactions between the *ortho*-hydrogen atoms in planar (D_{2h}) biphenyl, which is a transition state for rotation about the central carbon–carbon bond. The equilibrium geometry of biphenyl has a twisted (C_2) structure with a dihedral angle of 44.4° between the phenyl rings.[10] Bader and co-workers suggested[4] that, in the planar transition state of biphenyl, there is a bond with an associated stabilizing interaction between the *ortho*-hydrogen atoms. The strength of the H–H bond was calculated at the HF/6–311++G(2d,2p) level as 15.8 kcal mol^{-1}. This is in conflict with the traditional explanation for the rotational barrier for biphenyl, which suggests there is steric repulsion and no attraction between the *ortho*-hydrogen atoms in the transition state.

The heretical suggestion of Bader and co-workers[4] was criticized by Poater, Solá, and Bickelhaupt (PSB-1)[7] who advocated the classical explanation for the rotational barrier. PSB-1 stated that hydrogen–hydrogen bonding in planar biphenyl does not exist. The authors carried out an energy decomposition analysis (EDA) of the interactions between the phenyl rings of biphenyl as a function of the dihedral angle. PSB-1 found that the steric repulsion between the phenyl moieties indeed decreases by 6.9 kcal mol^{-1} when one goes from the C_2 equilibrium geometry to the D_{2h} transition state. However, the authors noted that the central C1–C7 bond between the phenyl rings in the transition state is about 0.01 Å longer than at equilibrium. EDA calculations of the rotational profile where the central C1–C7 bond length is kept frozen at the equilibrium value give an increase in the steric repulsion at the transition state. PSB-1 concluded from this finding that the steric repulsion between *ortho*-hydrogen atoms is the actual driving force for the rotational barrier and for the lengthening of the central C1–C7 bond.[7] The reasoning of PSB-1[7] received a rebuttal by Bader,[8] which in turn was replied by Poater, Solá, and Bickelhaupt in a second paper (PSB-2).[9]

A critical examination of the findings of Bader and co-workers[4] and those of PSB-1[7] reveals that the results of the two studies actually complement and even agree with each other, and that the divergence comes from the interpretation of the results. The AIM study shows that while the energies of the atomic basins of the *ortho*-hydrogen atoms in biphenyl *decrease* in the planar transition state relative to the minimum structure, the energies of the atomic basins of the central carbon atoms C1 and C7 *increase* by 32.6 kcal mol^{-1}, whereas the energies of the remaining carbon atoms decrease by 9.4 kcal mol^{-1}.[4] Thus, with the geometry change from the energy minimum to the transition state of the molecule there is a concomitant alteration of the energies of the atomic basins, which exhibit a stabilization of the *ortho*-hydrogen atoms and a destabilization of the central carbon atoms. This is in agreement with the EDA calculations of PSB-1 using the optimized geometries.[7] Bader and co-workers conclude from their analysis of the energy changes of the atomic basins of biphenyl: "The formation of the H–H interactions admittedly causes an increase in the separation between the two rings, one that results in an increase in the energy of atoms C1 and C7 linking the rings."[4] But the increase of the C1–C7 bond length and the concomitant energy increase of the atomic basins is enforced by the *ortho*-hydrogen atoms which would otherwise exhibit strong repulsion, yielding an even higher rotational barrier. The findings of Bader and co-workers that the atomic basins of the *ortho*-hydrogen atoms become significantly stabilized in the planar transition state, yielding a bond path, is thus justified because it is supported by the calculated data. However, the traditional explanation for the rotational barrier holds because the driving force for the calculated changes in the energies and in the electronic structure is the (avoided) repulsion between the *ortho*-hydrogen atoms. Furthermore, the H–H bond path which is found in the planar transition

state of biphenyl should *not* be considered a chemical bond because, following the IUPAC definition, it does not lead to a species which has sufficient stability to make it convenient for the chemist to consider it as an independent molecular species. The D_{2h} form of biphenyl is a transition state but not an energy minimum. Chemistry is primarily concerned with molecules but not with atoms in molecules. Chemical bonds are convenient constructions that are defined for helping chemists to distinguish between different molecules and to explain chemical reactions in terms of the breaking and making of bonds. This unicorn-type appearance[11] of chemical bonding is characteristic for chemistry, which often uses loosely defined models that are useful for explaining trends in chemical reactivity and molecular structure, and may therefore sometimes lead to controversial discussions.[12]

The situation becomes more complicated when the second example, which has been discussed with opposing viewpoints in the recent literature, is considered. In 2004, Haaland and co-workers[5] reported a theoretical study of the inclusion complex of a helium atom in $C_{10}H_{16}$ adamantane He@adam (Scheme 1), which is a minimum on the potential energy surface (PES). The topological analysis of He@adam shows that there are bond paths between He and the four carbon atoms carrying one hydrogen atom He–CH, which according to the AIM theory suggests that there are four helium–carbon bonds. However, the complex He@adam was calculated by Haaland and co-workers[5] to be 154.2 kcal mol^{-1} higher in energy than free adamantane + He, which indicates that the helium–adamantane interactions are destabilizing overall. The barrier for helium dissociation where He passes through one of the C_6 rings was calculated to be 41.1 kcal mol^{-1}. Examination of the AIM data showed that the energy of the helium atom in He@adam decreases by 301.9 kcal mol^{-1} relative to a free He atom. The energy of the carbon atoms connected to He by a bond path increase by 4×52.1 kcal mol^{-1} = 208.4 kcal mol^{-1}, which means that there is a net stabilization of the C_4He moiety of -93.5 kcal mol^{-1}. Nevertheless, the authors dismissed the notation of a He–C chemical bond in He@adam using the following definition: "Most chemists would probably agree that the defining property of a chemical bond is the existence of a positive bond rupture energy, that is, that the energy of the molecule is lower than the energy of the fragments, and this is the definition adopted in this paper."[5]

We very much hope that there are *not* many chemists who will agree with the above definition, because otherwise many interesting molecules would suddenly be considered not to have a chemical bond. This holds, for example, for experimentally known high-energy compounds like fluoroazide, FN_3, where the bond rupture $FN_3 \rightarrow FN + N_2$ is calculated to be exothermic by approximately -25 kcal mol^{-1}.[13] It holds particularly for doubly and more highly charged cations that are often metastable, that is, they are local minima on the PES although the dissociation into singly charged fragments is exothermic.[14] A pertinent example is He_2^{2+}, which was already predicted to be metastable by Pauling in 1933.[15] The prediction was later confirmed by experimental[16] and theoretical[17] studies, which give a calculated well depth at the full-CI level of 32.6 kcal mol^{-1} and a short equilibrium distance of 0.7025 Å, leaving no doubt that there is a chemical bond in He_2^{2+}. The calculations also showed that the dication is thermodynamically unstable with respect to dissociation into 2 He^+ by 199.9 kcal mol^{-1}. Another example relevant to the present study is the isoelectronic helium analogue of acetylene, $HeCCHe^{2+}$. Quantum-chemical calculations predict that the latter dication has a $^1\Sigma_g^+$ ground state, which is a minimum on the PES possessing very short He–C (1.085 Å) and C–C (1.197 Å) bonds.[18] Although the calculated carbon–carbon distance in $HeCCHe^{2+}$ is even shorter than in HCCH (1.217 Å), rupturing the C–C bond in the dication to yield two CHe^+ cations is thermodynamically unstable by 112.6 kcal mol^{-1}.

The nature of the interatomic interactions in He@adam and other caged species E@adam (E = Ne, Li^+, Be^{2+}, B^{3+}, Al^{3+}) was recently analyzed with the AIM theory by Bader and Fang (BF).[6] Their findings were in agreement with the results of Haaland et al[5] for He@adam but the conclusion was different. BF argued that there is no repulsion between the helium and carbon atoms connected by a He–C bond path, because the atoms are energetically stabilized with respect to the free atoms. The overall energy increase of the complex comes from the higher energies of the other carbon and from the hydrogen atoms. The analysis of the bond critical point data shows that the critical indices of the He–C interactions, ρ_b, $\nabla^2\rho_b$, and H_b, are intermediate between closed-shell and electron-sharing interactions resembling the values for a transition metal–carbonyl bond. BF therefore suggest that the He–C interactions in He@adam should be considered a chemical bond.[6] Since He@adam is an energy-minimum structure and not a transition state like planar biphenyl the conclusion of BF appears reasonable.

The assignment of a He–C bond in He@adam suggested by BF[6] has been criticized in the second paper of Poater, Solá, and Bickelhaupt (PSB-2)[9] using different arguments from Haaland et al.[5] PBS-2 calculated a fragment of He@adam where one of the CH_2 groups was removed and the remaining open valences became saturated with hydrogen atoms. This effectively removes a bar from the cage which holds the helium atom inside He@adam. Geometry optimization of the latter complex with the helium atom inside the fragment leads to the dissociation of He. PSB-2 therefore concluded that there is no He–C bonding because the helium atom dissociates from the opened cage during the geometry optimization.[9] However, this finding is not a valid argument against the assignment of a He–C bond in intact He@adam, because the interatomic interactions in the broken up cage are not the same as in the complete complex. Moreover, it requires energy to distort the structure of He@adam in such a way that the helium atom dissociates. The minimum activation barrier for the process is 41.1 kcal mol^{-1}[5], which is quite high. He_2^{2+} requires less energy to dissociate in an exothermic process than He@adam. We want to point out that the 1997 IUPAC definition[1b] of a

chemical bond does not say that there must be *attractive* forces between atoms or groups of atoms which *lead to the formation of an aggregation with sufficient stability to make it convenient for the chemist to consider it as an independent "molecular species"*. There is no doubt that He@adam is an independent molecular species.

The question about the nature of the interatomic interactions of caged atoms is not confined to molecules which belong to the realm of computational chemistry. He@adam may seem exotic but we want to point out that a complex where a helium atom is inside a $C_{20}H_{20}$ dodecahedrane cage has already been synthesized.[19] Calculations at MP2/6–311G(d,p) suggest that the complex $He@C_{20}H_{20}$ is 33.8 kcal mol^{-1} higher in energy than $He + C_{20}H_{20}$.[20] DFT calculations at the B3LYP/6–311G(d,p) level give an even larger value for the inclusion energy of 37.5 kcal mol^{-1},[20] which slightly increases to 37.9 kcal mol^{-1} when diffuse functions are added at the B3LYP/6–311+G(d,p) level.[21]

In this paper we report on quantum-chemical investigations of noble gas dimers Ng_2 (Ng = He–Xe) confined in a C_{60} cage. We wanted to know how the valence electrons of atoms which have a fully occupied valence shell change when they are confined to strong interatomic interactions at equilibrium geometry. The theoretical data are exciting because they suggest that there may be a new type of interatomic interaction, which would provide material for further stimulating discussions about the nature of a chemical bond. The lightest homologue, $He_2@C_{60}$, has been experimentally observed.[22] It has also been the subject of theoretical studies focusing mainly on the ^{3}He NMR chemical shift of $He_2@C_{60}$.[23] There is agreement between the results of the quantum-chemical calculations and the interpretation of the NMR experiments, that the helium atoms move freely in the cage and that the ^{3}He NMR chemical shift of $He_2@C_{60}$ is approximately the same as in $He@C_{60}$. The next heavier homologue $Ne_2@C_{60}$ and the mixed species $HeNe@C_{60}$ may have also been observed in experiment, although a definitive identification could only be made for $Ne_2@C_{70}$ and $HeNe@C_{70}$ using the heavier NMR active isotope ^{22}Ne.[24] The heavier homologues $Ar_2@C_{60}$, $Kr_2@C_{60}$, and $Xe_2@C_{60}$ have not been observed so far. Except for $He_2@C_{60}$[23] and $Ne_2@C_{60}$[23b] there is no theoretical study about noble gas complexes $Ng_2@C_{60}$ known to us. Endohedral complexes with one noble gas atom inside a fullerene cage $Ng@C_{60}$ have been observed for all noble gas atoms Ng = He–Xe.[25]

Finally we want to emphasize that the present work touches only some aspects of the chemical bond. A thorough analysis of the nature of the chemical bond aiming at a physical understanding of electron-sharing chemical bonds was recently given by Bitter, Ruedenberg, and Schwarz.[26]

Methods

The geometries of the molecules were optimized by using density functional theory (DFT) at the BP86[27] level using the RI (resolution of the identity) approximation[28] in conjunction with the Weigend/Ahlrichs all-electron basis sets def2-TZVPP[29] for all atoms except Xe. For xenon we employed a quasi-relativistic effective core potential (ECP) combined with a TZVPP valence basis set.[30] This level of theory is denoted as BP86/TZVPP. The vibrational frequencies were calculated at this level of theory. We also calculated the energies of the BP86/TZVPP optimized structures using Møller–Plesset perturbation theory terminated at second order (MP2)[31] in conjunction with the above TZVPP valence basis sets. Single-point energy calculations were also performed by using the spin-component-scaled MP2 method (SCS-MP2) proposed by Grimme,[32] which has been proven to give highly accurate energies for large main-group compounds.[33] The results of the SCS-MP2/TZVPP calculations are used as a reference for the accuracy of the theoretically predicted energies in this work. The calculated reaction energies were corrected for the basis-set superposition error (BSSE) using the counterpoise method suggested by Boys and Bernardi.[34] The geometry and energy calculations were carried out with the program package Turbomole.[35] The density used for the AIM analysis of the Xe-containing compounds was taken from a BP86 single-point calculation with an all electron basis set of TZVPP-quality of Ahlrichs.[36]

The electronic structure of the molecules was analyzed with different methods. For the charge distribution we used the natural bond orbital (NBO) method of Weinhold.[37] We also carried out an AIM analysis of the electron density distribution developed by Bader.[38] For the latter we used the program package AIMPAC.[39] Finally, we investigated for some molecules the interatomic interactions between Ng_2 and C_{60} using an energy decomposition analysis (EDA).[40] The EDA calculations of the BP86/TZVPP optimized structures were performed at the BP86 level using uncontracted Slater-type orbitals (STOs) which have TZ2P quality.[41] The latter calculations were carried out with the program package ADF.[42]

The focus of the EDA bonding analysis[43] is the instantaneous interaction energy ΔE_{int}, which is the energy difference between the molecule and the fragments Ng_2 and C_{60} with the frozen geometry of $Ng_2@C_{60}$. The interaction energy is divided into three main components, as given in Equation (1).

$$\Delta E_{int} = \Delta E_{elstat} + \Delta E_{Pauli} + \Delta E_{orb} \quad (1)$$

The term ΔE_{elstat} gives the electrostatic interaction energy between the fragments, which is calculated with a frozen density distribution in the geometry of the complex. The Pauli repulsion (ΔE_{Pauli}) arises as the energy change associated with the transformation from the superposition of the unperturbed electron densities of fragments $\rho_A + \rho_B$ to the wavefunction $\Psi^0 = N\hat{A}\{\Psi_A \cdot \Psi_B\}$, which properly obeys the Pauli principle through explicit antisymmetrization ($\hat{A}$) and renormalization (N) of the product wavefunction. It comprises the destabilizing interactions between electrons on either fragment with the same spin. The stabilizing orbital

interaction term ΔE_{orb} is calculated in the final step of the analysis when the orbitals relax to their final form. The latter can be decomposed into contributions from each irreducible representation of the point group of the interacting system. This is very helpful because it directly gives the stabilization that comes from orbitals with different symmetries. To obtain the bond dissociation energy (BDE) one has to consider the preparation energy ΔE_{prep}, which is the energy difference of the fragments Ng_2 and C_{60} between their equilibrium geometry and the geometry which they have in the molecule, as shown in Equation (2).

$$\Delta E\ (=-\mathrm{BDE}) = \Delta E_{int} + \Delta E_{prep} \quad (2)$$

Since free Ng_2 dissociates into 2 Ng the preparation energy includes the formation of the noble gas dimer from two Ng atoms.

Geometries and energies: We optimized the geometries of $Ng_2@C_{60}$ at the BP86/TZVPP level using different symmetry constraints, which are shown in Figure 1. In the D_{5d} structure the Ng–Ng axis is oriented along the connecting line between the midpoints of two opposing five-membered rings of the C_{60} cage, while in the D_{3d} geometry it is oriented along the axis between the midpoints of two opposing six-membered rings. Finally, in the D_{2h} structure the Ng–Ng axis lies along the connecting line between the midpoints of two opposing C–C bonds of six-membered rings that are facing each other. Table 1 gives the most important interatomic distances and the relative energies of the optimized structures.

Table 1. Calculated interatomic distances [Å] and relative energies [kcal mol^{-1}] of the D_{5d}, D_{3d}, and D_{2h} structures of $Ng_2@C_{60}$.

	Ng	r(Ng–Ng)	r(Ng–C) (shortest)	r(C–C) (shortest)	r(C–C) (longest)	E_{rel} (BP86)	E_{rel} (MP2)[a]	E_{rel} (SCS-MP2)[a]
D_{5d}	He	1.948	2.671	1.399	1.455	−0.02	0.05	0.05
	Ne	2.095	2.632	1.398	1.459	0.21	0.30	0.26
	Ar	2.361	2.608	1.395	1.477	0.83	1.17	0.97
	Kr	2.458	2.616	1.395	1.489	1.18	1.72	1.27
	Xe	2.494	2.598	1.402	1.500	0.55	−2.84	−3.97
D_{3d}	He	1.953	2.696	1.398	1.455	0.00	0.00	0.00
	Ne	2.099	2.657	1.397	1.458	0.00	0.00	0.00
	Ar	2.364	2.630	1.391	1.473	0.00	0.00	0.00
	Kr	2.460	2.637	1.389	1.481	0.00	0.00	0.00
	Xe	2.494	2.633	1.391	1.480	0.00	0.00	0.00
D_{2h}	He	1.951	2.617	1.398	1.455	−0.02	−0.07	−0.02
	Ne	2.098	2.578	1.396	1.460	0.07	−0.06	0.07
	Ar	2.364	2.563	1.389	1.478	0.36	0.34	0.36
	Kr	2.460	2.578	1.385	1.490	0.77	0.84	0.77
	Xe	2.491	2.547	1.386	1.493	0.86	0.99	0.86

[a] Using BP86 optimized geometries. A TZVPP basis set was always employed.

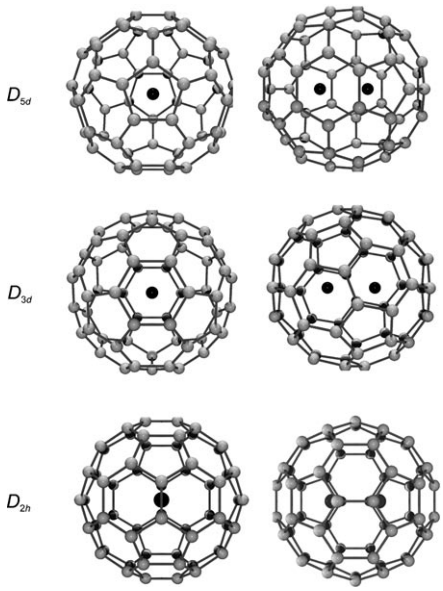

Figure 1. Graphical display of the D_{5d}, D_{3d}, and D_{2h} structures of the calculated $Ng_2@C_{60}$ molecules. Two perspectives are shown for each structure.

The calculated energies shown in Table 1 indicate that the structures that possess D_{5d}, D_{3d}, and D_{2h} symmetry are very close in energy. The BP86/TZVPP calculations predict that the most stable $Ng_2@C_{60}$ compounds have D_{3d} symmetry when Ng = Ne, Ar, Kr, Xe, while the D_{2h} and D_{5d} structures of $He_2@C_{60}$ are 0.02 kcal mol^{-1} lower in energy than the D_{3d} form, which is irrelevant. Single-point energy calculations at MP2/TZVPP and SCS-MP2/TZVPP using the BP86/TZVPP optimized geometries predict similar energy differences between the structures as using BP86/TZVPP, except for $Xe_2@C_{60}$. The ab initio calculations suggest that the D_{5d} structure of $Xe_2@C_{60}$ is the global energy minimum, which is, at the SCS-MP2/TZVPP level, 3.97 kcal mol^{-1} (2.84 kcal mol^{-1} at MP2/TZVPP) lower in energy than the D_{3d} form. The BP86/TZVPP calculations give the latter isomer as 0.55 kcal mol^{-1} more stable than the former structure. Except for $Xe_2@C_{60}$ the DFT and ab initio calculations give energy differences of <2 kcal mol^{-1} between the D_{5d}, D_{3d}, and D_{2h} forms of $Ng_2@C_{60}$. The calculations of the harmonic frequencies at BP86/TZVPP gave some small imaginary modes, which may arise from tiny maxima on the potential energy surface, or may come from numerical integration using a finite grid. Calculations of $Ng_2@C_{60}$ without symmetry constraints gave structures which are <0.1 kcal mol^{-1} lower in energy than the D_{3d} or D_{5d} species, which means that the latter structures can be considered as the equilibrium geometries. We conclude that there is a nearly free precession movement of diatomic Ng_2 around its midpoint in the C_{60} cage, with the pos-

sible exception of the Xe_2 dimer. The symmetry assignments for a frozen equilibrium structure are therefore not really relevant for $Ng_2@C_{60}$ at room temperature.

The calculated geometries show (Table 1) that the Ng–Ng equilibrium distances in $Ng_2@C_{60}$ are as expected to be significantly shorter than the long Ng–Ng bonds of free Ng_2, which are weakly bonded van der Waals complexes. Recent high level ab initio calculations give equilibrium distances for the free dimers: r(He–He) = 2.977, r(Ne–Ne) = 3.099, r(Ar–Ar) = 3.779, r(Kr–Kr) = 4.04, r(Xe–Xe) = 4.42 Å.[44] The calculated values for the lighter dimers are in excellent agreement with experimental values: r(He–He) = 2.970, r(Ne–Ne) = 3.091, r(Ar–Ar) = 3.757 Å.[45] It is noteworthy that the theoretically predicted Xe–Xe bond length in $Xe_2@C_{60}$, r(Xe–Xe) = 2.494 Å, is much shorter even than the experimental distance in the Xe_2^+ ion, r(Xe–Xe) = 3.087 Å, which has been measured by X-ray structure analysis.[46] The calculated value at BP86/TZVPP for the latter cation is r(Xe–Xe) = 3.228 Å. According to the calculations the C–C distances in $He_2@C_{60}$ and $Ne_2@C_{60}$ (Table 1) are hardly distorted compared to free C_{60}. The BP86/TZVPP optimization of C_{60} (I_h symmetry) gives for the shortest C–C bond the value r(C–C) = 1.399 Å and for the longest C–C bond the value r(C–C) = 1.454 Å. Larger changes of the C–C distances are calculated for the heavier homologues $Ar_2@C_{60}$ and $Kr_2@C_{60}$, and particularly $Xe_2@C_{60}$. Note that the shorter C–C bond in free C_{60} becomes even slightly shorter in $Ng_2@C_{60}$ except for the D_{5d} structure of $Xe_2@C_{60}$, while the longer C–C bond becomes elongated upon uptake of Ng_2 as expected.

It is interesting to estimate the maximum distance available in free C_{60} to accommodate the Ng_2 species. The calculated diameter for the empty fullerene is 6.664 Å (distance between two C_5 rings along one C_5 axis in C_{60} (I_h)). The van der Waals radius of carbon may be taken as 1.7 Å, which leaves a distance of about 3.3 Å for the noble gas dimer. The above values for the equilibrium distances in free Ng_2 indicate that the uptake of He_2 and Ne_2 into the C_{60} cage induces only weak steric repulsion, while the inclusion of the heavier homologues should encounter strong repulsive interactions.

Table 2 shows calculated reaction energies that are important for the present study. The first set of values for reactions 1 Ng gives the energies which are necessary to bring two Ng atoms as close to each other as in $Ng_2@C_{60}$. The brackets in [Ng_2] indicate that the noble gas dimer has the frozen bond length as calculated in $Ng_2@C_{60}$. The positive reaction energies strongly increase from [He_2] which has D_e = 1.59 kcal mol^{-1} to [Xe_2], where the Xe–Xe interactions are 109.81 kcal mol^{-1} repulsive (SCS-MP2/TZVPP). Note that the BP86/TZVPP and MP2/TZVPP values for reactions 1 Ng are not very different from the SCS-MP2/TZVPP results. Reactions 2 Ng give the complementary relaxation energies of the cage [C_{60}], which are calculated with the frozen geometry of $Ng_2@C_{60}$ yielding C_{60} at its equilibrium geometry. The values at BP86/TZVPP and MP2/TZVPP again differ by less than 4 kcal mol^{-1} from the SCS-MP2/TZVPP data.

Reactions 3 Ng give the interaction energies between the [Ng_2] species and the cage [C_{60}]. The SCS-MP2/TZVPP method gives repulsive interaction energies, which range at the BSSE corrected SCS-MP2/TZVPP level from 1.26 kcal mol^{-1} for $He_2@C_{60}$ to 157.21 kcal mol^{-1} for $Xe_2@C_{60}$. We wish to point out that the BSSE corrected BP86/TZVPP

Table 2. Calculated reaction energies for (D_{3d}) Ng2@C60 [kcal mol^{-1}].

	No	BP86	MP2[a]	SCS-MP2[a]
2 Ng → [Ng_2][c]	1He	2.07	1.54	1.59
	1Ne	6.38	5.52	5.65
	1Ar	30.38	30.48	31.76
	1Kr	48.86	50.82	56.06
	1Xe	102.26	105.65	109.81
C_{60} → [C_{60}][d]	2He	0.02	0.29	0.20
	2Ne	0.79	1.62	1.34
	2Ar	11.48	14.65	13.66
	2Kr	23.68	28.59	27.16
	2Xe	34.40	39.08	38.46
[Ng_2][c] + [C_{60}][d] → [$Ng_2@C_{60}$][b]	3He	7.47 (*8.14*)	−1.84 (*−0.58*)	−0.05 (*1.26*)
	3Ne	20.13 (*22.20*)	1.45 (*6.92*)	5.44 (*10.83*)
	3Ar	83.84 (*86.17*)	22.26 (*33.25*)	40.06 (*51.25*)
	3Kr	135.48 (*138.28*)	54.92 (*68.61*)	80.16 (*94.34*)
	3Xe	201.29 (*203.48*)	80.45 (*112.45*)	125.94 (*157.21*)
2 Ng + C_{60} → [$Ng_2@C_{60}$][b]	4He	9.56 (*10.23*)	−0.01 (*1.25*)	1.74 (*3.05*)
	4Ne	27.30 (*29.37*)	8.59 (*14.06*)	12.43 (*17.82*)
	4Ar	125.70 (*128.03*)	67.39 (*78.38*)	85.48 (*96.67*)
	4Kr	208.02 (*210.82*)	134.33 (*148.02*)	163.38 (*177.56*)
	4Xe	337.95 (*340.14*)	225.18 (*257.18*)	274.22 (*305.49*)

[a] Using BP86 optimized geometries. A TZVPP basis set was always employed. [b] Values in *italics* are counterpoise corrected for the BSSE. [c] [Ng_2] means the Ng_2 dimer with the Ng–Ng distance in $Ng_2@C_{60}$. [d] [C_{60}] means the C_{60} cage with the geometry in $Ng_2@C_{60}$.

values for reactions 3 Ng suggest a much stronger repulsion, from 8.14 kcal mol^{-1} for $He_2@C_{60}$ to 203.48 kcal mol^{-1} for $Xe_2@C_{60}$, while the repulsion at the BSSE corrected MP2/TZVPP level is significantly weaker than at SCS-MP2/TZVPP. The BSSE corrected MP2/TZVPP value for $He_2@C_{60}$ is even weakly attractive (−0.58 kcal mol^{-1}). The calculated data show that the BSSE corrections of the MP2/TZVPP and SCS-MP2/TZVPP values are much larger than for the BP86/TZVPP data.

The large differences clearly show that not only the DFT values but also the MP2/TZVPP data for the interaction energies between Ng_2 and C_{60} are not reliable. Reactions 4 Ng finally give the dissociation energies of $Ng_2@C_{60}$ yielding the relaxed cage C_{60} and two Ng atoms as products. The calculated values are the sum of the reaction energies for reactions 1 Ng–3 Ng. The decomposition of the endohedral fullerenes at the BSSE-corrected SCS-MP2/TZVPP level is endothermic, between 3.05 kcal mol^{-1} for $He_2@C_{60}$ and 305.49 kcal mol^{-1} for $Xe_2@C_{60}$. The BSSE corrected BP86/TZVPP values suggest even higher relative energies for $Ng_2@C_{60}$ of between 10.23 kcal mol^{-1} for $He_2@C_{60}$ and 340.14 kcal mol^{-1} for $Xe_2@C_{60}$, while the BSSE corrected MP2/TZVPP calculations give smaller values, between 1.25 kcal mol^{-1} for $He_2@C_{60}$ and 257.18 kcal mol^{-1} for $Xe_2@C_{60}$. All methods agree that the heavier endohedral fullerenes $Ar_2@C_{60}$, $Kr_2@C_{60}$, and $Xe_2@C_{60}$ are high-energy compounds which are thermodynamically unstable toward the loss of two noble gas atoms.

It is interesting to compare our results with a previous theoretical study of the compounds $Ng@C_{60}$ (Ng = He–Xe) by Bühl et al.[47] The calculations at MP2 using DZP quality basis sets showed that the latter endohedral fullerenes are thermodynamically stable toward loss of the noble gas atom.[48] The calculated interaction energies at MP2/DZP without BSSE correction are between −1.0 kcal mol^{-1} for $He@C_{60}$ and −17.1 kcal mol^{-1} for $Xe@C_{60}$. The BSSE corrected values range between −0.3 kcal mol^{-1} for $He@C_{60}$ and −5.4 kcal mol^{-1} for $Xe@C_{60}$.[47] The results indicate that the steric repulsion in $Ng@C_{60}$ is compensated by a weak van der Waals attraction.[49]

Bonding analysis: The central topic of the bonding analysis concerns the nature of the Ng–Ng and Ng–C interactions. In particular, we want to address the question of whether the latter interactions should be considered as genuine chemical bonds. The IUPAC definition of a chemical bond, cited in the introduction, gives a straightforward answer in the affirmative. Without calculating the activation energy for opening the C_{60} cage of $Ng_2@C_{60}$ for releasing the encapsulated noble gas atoms, it can be stated that the barrier is certainly high enough to provide sufficient stability to observe and to identify the endohedral fullerenes. The crucial question from an experimental point will be the synthesis of $Ng_2@C_{60}$.

What about the forces acting on the noble gas atoms in $Ng_2@C_{60}$? Figure 2 shows the calculated potential well of the endohedral fullerenes as a function of the Ng–Ng distance. It is obvious that the noble gas atoms vibrate around an energy minimum, which for the heavier species Ar_2, Kr_2, and Xe_2 is very deep. Table 3 gives the calculated force constants k for the Ng–Ng stretching mode of $Ng_2@C_{60}$. The theoretical values for Ng = Ar, Kr, Xe are higher than the force constant for the C–C stretching mode in ethane. The latter value calculated at BP86/TZVPP is $k = 428.7$ N m^{-1}. It is evident that the well depth and the large force constants of Ng_2 in $Ng_2@C_{60}$ are enforced by the fullerene cage, but it is a matter of taste to dismiss this as a valid driving force for enforcing a chemical bond. Furthermore, the following discussion will show that the interactions between Xe_2 and C_{60} exhibit surprising features that only come to the fore by analyzing the electronic structure.

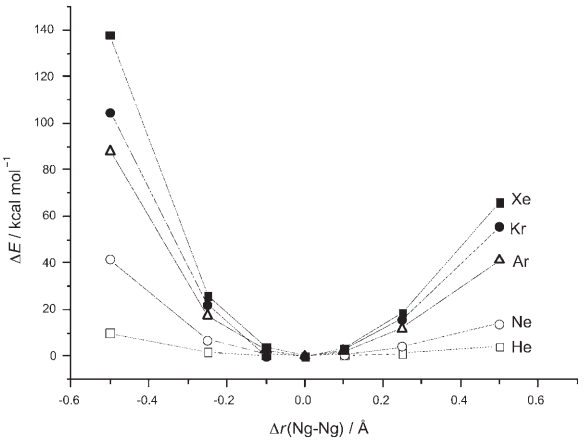

Figure 2. Calculated potential wells for the Ng–Ng stretching mode of D_{3d} $Ng_2@C_{60}$ at BP86/TZVPP.

Table 3. Calculated force constants k at BP86/TZVPP for the Ng–Ng stretching mode in (D_{3d}) Ng2@C60.

Ng	k [N m^{-1}]
He	37.8
Ne	146.3
Ar	443.0
Kr	603.9
Xe	708.9

To investigate the nature of the interatomic interactions in $Ng_2@C_{60}$ in more detail, we used several methods for analyzing the electronic structure of the endohedral fullerenes. We begin the discussion with the presentation of the results of the AIM analysis. Figure 3 shows the contour line diagrams for the Laplacian of the electron density $\nabla^2\rho(\mathbf{r})$ which were calculated for the D_{3d} structures of $Kr_2@C_{60}$ and $Xe_2@C_{60}$.[50]

The AIM analysis of (D_{3d}) $Kr_2@C_{60}$ and $Xe_2@C_{60}$ indicates that there is a Ng–Ng bond path and that there are also six Ng–C bond paths in the endohedral fullerenes. Two Ng–C bond paths for each noble gas atom are displayed in Figure 3 a and b, which show the Laplacian in one of the three σ_d molecular planes containing the noble gas atoms and four

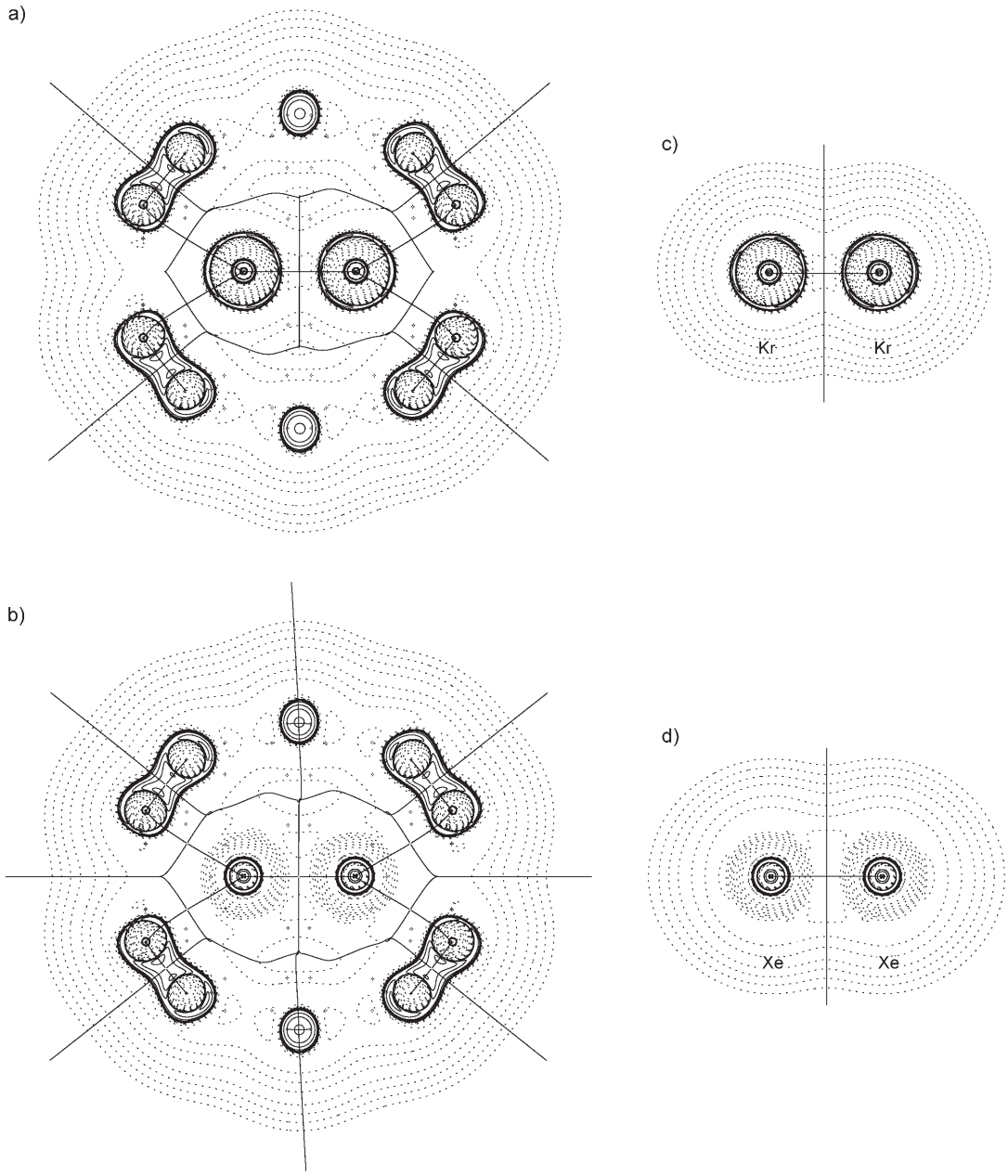

Figure 3. Contour line diagrams $\nabla^2\rho(r)$ of: a) $Kr_2@C_{60}$; b) $Xe_2@C_{60}$; c) $[Kr_2]$; d) $[Xe_2]$. Solid lines indicate areas of charge concentration ($\nabla^2\rho(r)<0$), while dashed lines show areas of charge depletion ($\nabla^2\rho(r)>0$). The thick solid lines connecting the atomic nuclei are the bond paths. The thick solid lines separating the atomic basins indicate the zero-flux surfaces crossing the molecular plane.

carbon atoms. The same situation is found for $Ar_2@C_{60}$, while the AIM analysis of the lighter D_{3d} homologues $He_2@C_{60}$ and $Ne_2@C_{60}$ gives only three Ng–C_2 paths connecting the Ng atoms with the midpoint of a C–C bond, yielding a local T-shape structure. The topography of the electron density thus suggests that the heavier noble gas atoms Ar, Kr, Xe are seven-coordinate in $Ng_2@C_{60}$, whereas the lighter atoms, He and Ne, are four-coordinate.

Further inspection of the Laplacian distribution shows significant differences between $Kr_2@C_{60}$ and $Xe_2@C_{60}$. There are three areas of local charge concentration ($\nabla^2\rho(r)<0$, solid lines) in the valence shell of the Kr atoms, while the valence shell of the Xe atoms exhibits a spherical area of charge depletion ($\nabla^2\rho(r)>0$, dashed lines). The shape of the Laplacian does not come from direct electronic interactions between Ng_2 and C_{60}. Figure 3c and d show the Laplacian distribution of free Ng_2 in the geometry of $Ng_2@C_{60}$, which is practically indistinguishable from the Laplacian distribution of the encapsulated Ng_2 species. The valence shell concentration of the $(5s)^2(5p)^6$ electrons of Xe_2 is too diffuse to appear as a local maximum of $\nabla^2\rho(r)$.

Table 4. Calculated values of the AIM analysis for the Ng–Ng, Ng–C, and C–C bonds of (D_{3d}) Ng2@C60 at BP86/TZVPP. Charge density at the bond critical point $\rho(r_b)$, Laplacian at the bond critical point $\nabla^2\rho(r_b)$, energy at the bond critical point $H(r_b)$.

Ng	Ng–Ng[a]			Ng–C			C–C		
	$\rho(r_b)$ [e Å^{-3}]	$\nabla^2\rho(r_b)$ [e Å^{-5}]	$H(r_b)$ [Hartree Å^{-3}]	$\rho(r_b)$ [e Å^{-3}]	$\nabla^2\rho(r_b)$ [e Å^{-5}]	$H(r_b)$ [Hartree Å^{-3}]	$\rho(r_b)$ [e Å^{-3}]	$\nabla^2\rho(r_b)$ [e Å^{-5}]	$H(r_b)$ [Hartree Å^{-3}]
He	0.094 (0.095)	2.165 (2.152)	0.040 (0.039)	0.060	1.042	0.017	1.882	−17.128	−1.773
Ne	0.215 (0.216)	6.107 (6.097)	0.062 (0.061)	0.103	1.860	0.022	1.866	−16.819	−1.746
Ar	0.418 (0.411)	6.235 (6.255)	−0.037 (−0.031)	0.204	2.827	0.009	1.805	−15.687	−1.640
Kr	0.479 (0.468)	5.548 (5.623)	−0.078 (−0.067)	0.247	2.950	−0.006	1.763	−14.957	−1.570
Xe	0.728 (0.671)	1.165 (3.386)	−0.341 (−0.284)	0.316	2.789	−0.038	1.723	−14.212	−1.505

[a] The values in parentheses give the results for free [Ng_2] using the Ng–Ng distance in the complex.

Table 4 gives the numerical results of the AIM calculations for the D_{3d} structures of $Ng_2@C_{60}$. The calculated values offer interesting insight particularly into the nature of the Ng–Ng and Ng–C interactions, which will be compared with the values for the C–C bonds. The calculated electron densities $\rho(r_b)$ and the negative values for the Laplacian $\nabla^2\rho(r_b)$ and for the energy $H(r_b)$ at the bond critical point r_b of the C–C bonds are typical for covalent bonds.[38,51] The smaller values for $\rho(r_b)$ and the positive values for the Laplacian, $\nabla^2\rho(r_b) > 0$, suggest that the Ng–Ng and Ng–C interactions should be classified as closed-shell type bonding.[38] The calculated $H(r_b)$ data which are positive or weakly negative agree with the classification of a closed-shell interaction except for the value of Xe_2. The rather large negative value $H(r_b) = -0.341$ Hartree Å^{-3} for the Xe–Xe bond indicates that the latter might be a shared-electron bond rather than a closed-shell interaction.[51] It has been shown previously that there are chemical bonds which have a positive value for the Laplacian although they are covalent electron-sharing bonds. A pertinent example is the F–F bond in F_2 which at HF/6–31G(d) has a positive Laplacian $\nabla^2\rho(r_b) = 2.908$ e Å^{-5} and a large negative value $H(r_b) = -2.045$ Hartree Å^{-3}.[51] This is the reason why the energy value at the bond critical point is considered a more reliable criterion to identify a shared-electron bond. Please note that a large negative energy value is already calculated for free [Xe_2] which has $H(r_b) = -0.284$ Hartree Å^{-3} (Table 4). Nevertheless, the AIM data for the Ng–Ng bond in $Ng_2@C_{60}$ and in free [Ng_2] differ most from each other when Ng = Xe.

The AIM data are a first hint that the bonding situation in $Xe_2@C_{60}$ may be different from that in the lighter homologues. A second indicator is the calculated charge distributions in the endohedral fullerenes, which are shown in Table 5. The atomic partial charge of the noble gas atoms is close to zero except for xenon. The rather large value of $q(Xe) = +0.53$ suggests that the [Xe_2] moiety in $Xe_2@C_{60}$ donates a significant amount of electronic charge (1.06 e) to the fullerene cage. The charge distribution indicates that the latter molecule may be better described in terms of the ionic species $Xe_2^+@C_{60}^-$. The breakdown of the charge distribution into the orbital occupation shows that the charge donation comes mainly from the occupied $5p_z$ valence orbitals of Xe, where z is the Xe–Xe bonding axis. This is reasonable because the highest occupied molecular orbital (HOMO) of Ng_2 is the σ* MO, which comprises the antibonding combination of the p_z AOs of Ng.

Table 5. NBO atomic partial charges and orbital occupations for the D_{3d} isomers of $Ng_2@C_{60}$ in the singlet ($^1A_{1g}$) state at BP86/TZVPP.

Ng	q(Ng)	ns	np_x	np_y	np_z
He	0.00	2.00	–	–	–
Ne	+0.01	2.00	2.00	2.00	2.00
Ar	+0.01	2.00	2.00	2.00	1.99
Kr	+0.03	2.00	1.99	1.99	1.97
Xe	+0.53	1.98	1.99	1.99	1.43

We analyzed the molecular orbitals of $Ng_2@C_{60}$ in more detail. Figure 4 shows the calculated energy levels of some relevant MOs. The σ* MO of [Ng_2], which is the HOMO of the free dimer, is the highest lying occupied a_{2u} orbital in the D_{3d} structure of $Ng_2@C_{60}$, except in $He_2@C_{60}$ and $Ne_2@C_{60}$ where one occupied a_{2u} cage orbital is higher in energy than the σ* MO of [Ng_2]. In the lighter complexes $He_2@C_{60}$, $Ne_2@C_{60}$, and $Ar_2@C_{60}$, the latter a_{2u} MO is energetically clearly lower lying than the HOMO of the endohedral fullerenes, which is the doubly degenerated e_u orbital. The a_{2u} σ*(Ng_2) MO is energetically much higher lying in the heavier homologues $Kr_2@C_{60}$ and $Xe_2@C_{60}$, where it becomes the HOMO of the molecules. Please note that the energy level of the a_{2u} HOMO in $Xe_2@C_{60}$ (−4.739 eV) is not very different from the energy level of the e_u LUMO (−4.524 eV) and the a_{2u} LUMO+1 (−4.359 eV).

It is enlightening to compare the calculated energy levels of the HOMO of [Ng_2] with the a_{2u} σ*(Ng_2) MO in $Ng_2@C_{60}$ and with the HOMO of free Ng. The calculated values are given in Table 6. The data show that there is a continuous increase in the rise of the HOMO energy when one goes from free Ng to [Ng_2]. Note that the $\Delta\varepsilon$ values [Ng_2]–Ng are rather small for helium (0.610 eV) and neon (0.949 eV) but they become significantly large for argon (2.062 eV), krypton (2.510 eV) and xenon (3.313 eV). The calculated changes in the energy level $\Delta\varepsilon$ σ*(Ng_2) when one goes from free [Ng_2] to $Ng_2@C_{60}$ show (Table 6) that the electron pairs of He_2 and Ne_2 become stabilized by the Coulomb interaction with the C_{60} cage, while the valence electron pairs of the a_{2u} σ*(Ng_2) MOs of Ar_2, Kr_2, and Xe_2 become destabilized. The overall destabilization of Ng_2 in $Ng_2@C_{60}$ comes from the steric repulsion which is caused by Pauli interactions.[49] This will be discussed below.

Figure 5 shows the frontier orbitals HOMO and LUMO and the nearest lying orbitals HOMO-1 and LUMO+1 of

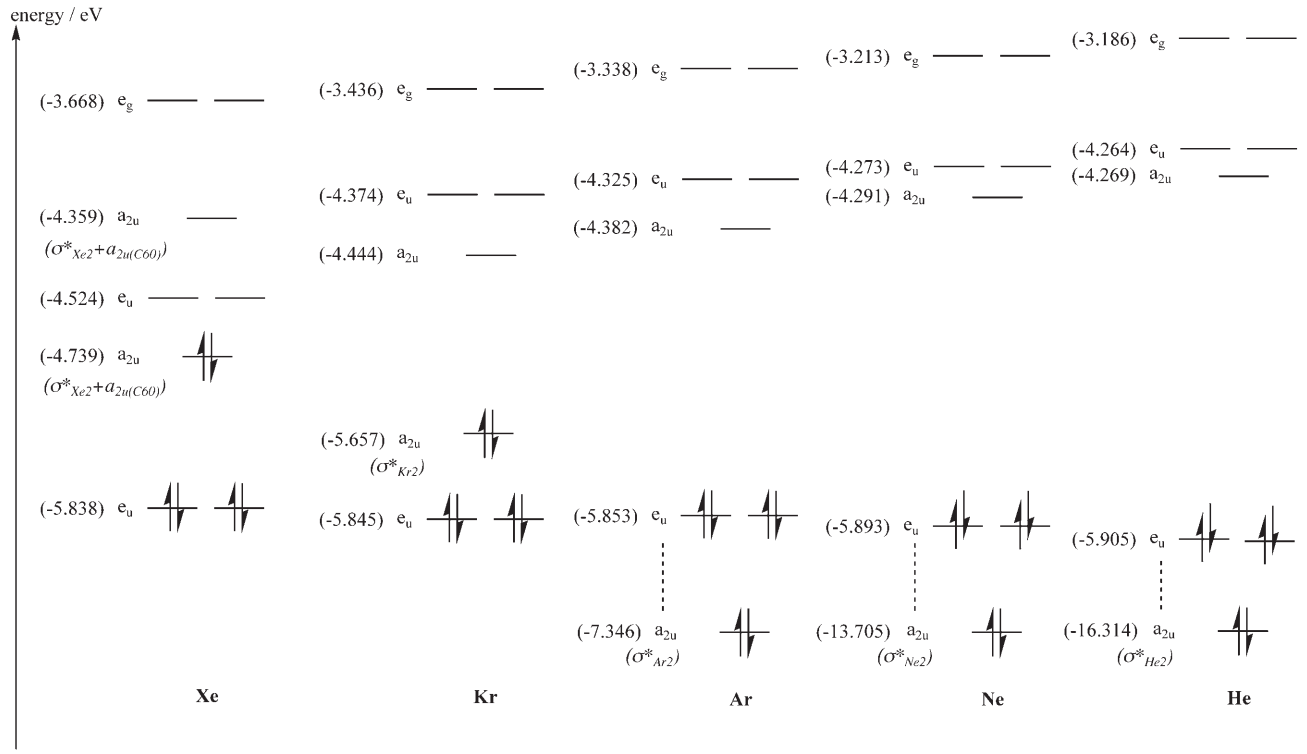

Figure 4. Energy levels of relevant occupied and vacant orbitals of $Ng_2@C_{60}$ in D_{3d} symmetry at BP86/TZVPP. The occupied a_{2u} orbitals are mainly the σ* HOMOs of $[Ng_2]$. The occupied e_u orbitals are mainly the highest lying C_{60} orbitals which are the HOMO for $He_2@C_{60}$, $Ne_2@C_{60}$, and $Ar_2@C_{60}$, but the HOMO-1 for $Kr_2@C_{60}$ and $Xe_2@C_{60}$.

Table 6. Calculated energy levels ε [eV] of the HOMO of Ng and $[Ng_2]$ and the occupied σ*(Ng_2) orbital in D_{3d} $Ng_2@C_{60}$ at BP86/TZVPP. Energy differences $\Delta\varepsilon$ between the orbitals.

Ng	ε_{HOMO} Ng	$\varepsilon(\sigma^*)_{HOMO}$ $[Ng_2]$	$\Delta\varepsilon_{HOMO}$ $[Ng_2]-Ng$	$\varepsilon(\sigma^*,Ng_2)$ $Ng_2@C_{60}$	$\Delta\varepsilon$ σ*(Ng_2) $Ng_2@C_{60}-[Ng_2]$
He	−15.793	−15.183	0.610	−16.314	−1.131
Ne	−13.291	−12.342	0.949	−13.705	−1.363
Ar	−10.297	−8.235	2.062	−7.436	0.889
Kr	−9.361	−6.851	2.510	−5.657	1.194
Xe	−8.319	−5.006	3.313	−4.739	0.267

$Kr_2@C_{60}$ and $Xe_2@C_{60}$. The e_u HOMO-1 orbital (only one component of the degenerate orbital is displayed) is the highest lying occupied orbital of the C_{60} cage, which has negligible contributions from the Ng_2 moiety. The latter orbital is the HOMO of $He_2@C_{60}$, $Ne_2@C_{60}$, and $Ar_2@C_{60}$. The remaining orbitals HOMO, LUMO, and LUMO+1 exhibit striking differences between $Kr_2@C_{60}$ and $Xe_2@C_{60}$. The a_{2u} HOMO of $Kr_2@C_{60}$ is mainly the (p_z-p_z) σ* MO of $[Kr_2]$, which has little contribution from the C_{60} cage. Contrary to the krypton compound the a_{2u} HOMO of $Xe_2@C_{60}$ shows a large mixing between the C_{60} orbitals and the (p_z-p_z) σ* MO of $[Xe_2]$. The shape of the latter orbitals explains the large positive partial charge of $[Xe_2]$ and the negative charge of C_{60} in the endohedral fullerene. The shape of the lowest lying vacant a_{2u} orbital of $Kr_2@C_{60}$ and $Xe_2@C_{60}$ is complementary to the HOMOs. The a_{2u} LUMO of $Kr_2@C_{60}$ comes from the C_{60} cage, which has negligible contributions from $[Kr_2]$, but the a_{2u} LUMO+1 of $Xe_2@C_{60}$ has a very large contribution from the (p_z-p_z) σ* MO of $[Xe_2]$. Note that the latter orbital is not the lowest lying vacant MO of $Xe_2@C_{60}$. The LUMO of $Xe_2@C_{60}$ is the degenerate e_u orbital which is mainly a C_{60} cage orbital. In the krypton compound it is the LUMO+1 (Figure 5).

The shape of the frontier orbitals and particularly the small HOMO-LUMO gap of $Xe_2@C_{60}$ poses the question of whether the calculated $^1A_{1g}$ state is the actual electronic ground state of the molecule. We therefore optimized the molecule in the electronic triplet state. The ordering of the frontier orbitals, as given in Figure 4, shows that this is not a trivial task because several triplet states must be considered, which may be close in energy. An accurate calculation of the electronic states would require multi-reference methods with large basis sets, which are not possible because of the size of the molecule. For the purpose of the present study it is sufficient, however, to estimate the relative energy of triplet states using single-reference methods. We therefore optimized at BP86/TZVPP the geometry of $Xe_2@C_{60}$ with a D_{3d} symmetry constraint in the $^3A_{1g}$ triplet state with the electron configuration $(e_u)^4(a_{2u})^1(a_{2u})^1(e_u)^0$, which is singly excited with respect to the $^1A_{1g}$ singlet state. The latter state has the electron configuration $(e_u)^4(a_{2u})^2(a_{2u})^0(e_u)^0$ (compare Figure 4). We also optimized the doubly excited ^3E_u triplet state,[52] which has the electron configration $(e_u)^4(e_u)^2(a_{2u})^0$. Table 7 gives the calculated energies.

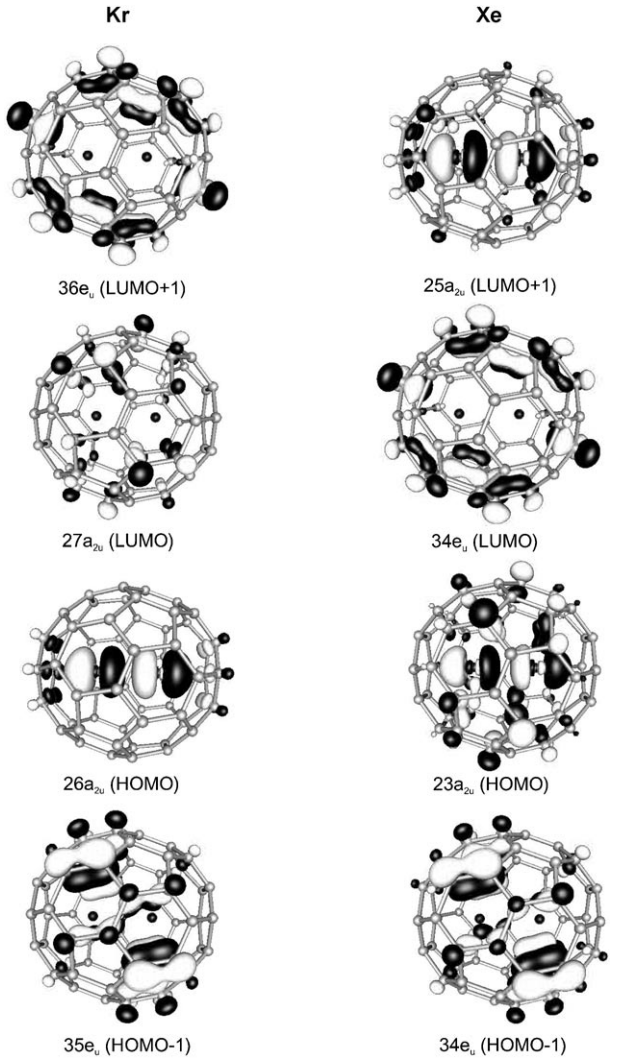

Figure 5. Plot of the frontier orbitals HOMO-1, HOMO, LUMO, and LUMO+1 of $Kr_2@C_{60}$ and $Xe_2@C_{60}$ at BP86/TZVPP.

Table 7. Calculated relative energies [kcal mol^{-1}] of (D_{3d}) $Xe_2@C_{60}$ in different electronic states.

	BP86	MP2[a]	SCS-MP2[a]
$..(e_u)^4(a_{2u})^2(a_{2u})^0(e_u)^0$ ($^1A_{1g}$)	0.00	0.00	0.00
$..(e_u)^4(a_{2u})^1(a_{2u})^1(e_u)^0$ ($^3A_{1g}$)	5.18	−3.39	−3.93
$..(e_u)^4(e_u)^2(a_{2u})^0(a_{2u})^0$ (^3E_u)	8.26	−8.93	−2.07

[a] Using BP86 optimized geometries. A TZVPP basis set was always employed.

At the BP86/TZVPP level, the singly excited $^3A_{1g}$ triplet state of $Xe_2@C_{60}$ is 5.18 kcal mol^{-1} higher in energy than the $^1A_{1g}$ singlet state, while the doubly excited ^3E_u triplet state is 8.26 kcal mol^{-1} above the singlet. The single-point energy calculations at the MP2/TZVPP//BP86/TZVPP level give a reverse stability order; the ^3E_u triplet is the most stable state of (D_{3d}) $Xe_2@C_{60}$, which is 8.93 kcal mol^{-1} lower than the $^1A_{1g}$ singlet, while the $^3A_{1g}$ triplet is 3.39 kcal mol^{-1} below the $^1A_{1g}$ state (Table 7). The more accurate SCS-MP2/TZVPP//BP86/TZVPP method predicts that the lowest lying electronic state is the $^3A_{1g}$ triplet state, which is 3.93 kcal mol^{-1} more stable than the $^1A_{1g}$ singlet state, while the ^3E_u triplet is 2.07 kcal mol^{-1} lower than the $^1A_{1g}$ singlet state. Please note that the SCS-MP2/TZVPP//BP86/TZVPP calculations predict that the D_{5d} structure of $Xe_2@C_{60}$ in the $^1A_{1g}$ singlet state is 3.97 kcal mol^{-1} lower in energy than the $^1A_{1g}$ singlet state of the D_{3d} geometry (Table 1). This means that, at the SCS-MP2/TZVPP//BP86/TZVPP level of theory, the $^1A_{1g}$ singlet state of the D_{5d} structure and the $^3A_{1g}$ triplet state of the D_{3d} structure of $Xe_2@C_{60}$ are energetically nearly degenerate. We did not calculate triplet states possessing D_{5d} geometry, nor did we calculate triplet states of lower symmetry, because the results suggest that several singlet and triplet states of $Xe_2@C_{60}$ are close in energy, which means that single-reference methods are not sufficient to reliably predict the lowest lying electronic state of the molecule. However, the calculations clearly show that, whatever the electronic ground state of $Xe_2@C_{60}$, the bonding in the complex should be considered in terms of interactions between a positively charged Xe_2^{q+} species and a negatively charged C_{60}^{q-} cage. Table 8 gives the atomic partial charges of Xe in $Xe_2@C_{60}$ at various electronic states. The calculated values indicate that the interacting species in the $^3A_{1g}$ triplet state and the $^1A_{1g}$ singlet state are singly charged $Xe_2^+ + C_{60}^-$, while the bonding in the ^3E_u triplet state is better discussed in terms of interactions between $Xe_2^{2+} + C_{60}^{2-}$. This is a qualitative reasoning. The calculated charges suggest intermediate situations where a charge flow takes place between the formally positively and negatively charged species.

Table 8. NBO atomic partial charges and orbital occupations for the D_{3d} isomers of $Xe_2@C_{60}$ in different electronic states at BP86/TZVPP.

State	q(Xe)	5s	5p$_x$	5p$_y$	5p$_z$
$..(e_u)^4(a_{2u})^2(a_{2u})^0(e_u)^0$ ($^1A_{1g}$)	+0.53	1.98	1.99	1.99	1.43
$..(e_u)^4(a_{2u})^1(a_{2u})^1(e_u)^0$ ($^3A_{1g}$)	+0.43	1.99	1.99	1.99	1.54
$..(e_u)^4(e_u)^2(a_{2u})^0(a_{2u})^0$ (^3E_u)	+0.76	1.98	1.99	1.99	1.20

Table 9 gives the theoretically predicted dissociation energies of singlet and triplet $Xe_2@C_{60}$, yielding neutral or charged fragments. The fragmentation into neutral products is strongly exothermic. The dissociation of $Xe_2@C_{60}$ into the singly charged species Xe_2^+ and C_{60}^- is still exothermic at the BSSE corrected MP2/TZVPP//BP86/TZVPP and SCS-MP2/TZVPP//BP86/TZVPP levels but much less so than the fragmentation reaction yielding neutral species. Note that the BP86/TZVPP calculations give exothermic reaction energies that are about 100 kcal mol^{-1} too high. All levels of theory predict that $Xe_2@C_{60}$ is thermodynamically stable toward dissociation into $Xe_2^{2+} + C_{60}^{2-}$.

We analyzed the electronic structure of Xe_2^+ and Xe_2^{2+} with the AIM method at the optimized Xe–Xe bond length and at the frozen distance taken from $Xe_2@C_{60}$. Table 10 gives the numerical results for Xe_2^{q+}. The data for Kr_2^{q+} are

Table 9. Calculated bond dissociation energies [kcal mol^{-1}] for $Xe_2@C_{60}$ (D_{3d}).[b]

	BP86/TZVPP	MP2/TZVPP[a]	SCS-MP2/TZVPP[a]
State		$Xe_2@C_{60} \rightarrow C_{60}+2\,Xe$	
$..(e_u)^4(a_{2u})^2(a_{2u})^0(e_u)^0$ ($^1A_{1g}$)	−337.95 (*−340.14*)	−225.18 (*−257.18*)	−274.22 (*−305.48*)
$..(e_u)^4(a_{2u})^1(a_{2u})^1(e_u)^0$ ($^3A_{1g}$)	−343.13 (*−345.36*)	−221.80 (*−254.01*)	−270.29 (*−301.81*)
$..(e_u)^4(e_u)^2(a_{2u})^0$ (^3E_u)	−346.21 (*−348.47*)	−216.26 (*−248.40*)	−272.15 (*−303.56*)
		$Xe_2@C_{60} \rightarrow C_{60}^- + Xe_2^+$	
$..(e_u)^4(a_{2u})^2(a_{2u})^0(e_u)^0$ ($^1A_{1g}$)	−154.71 (*−156.79*)	2.11 (*−27.65*)	−36.38 (*−65.37*)
$..(e_u)^4(a_{2u})^1(a_{2u})^1(e_u)^0$ ($^3A_{1g}$)	−159.89 (*−161.98*)	5.49 (*−24.29*)	−32.45 (*−61.56*)
$..(e_u)^4(e_u)^2(a_{2u})^0$ (^3E_u)	−162.97 (*−165.05*)	11.03 (*−18.75*)	−34.32 (*−63.25*)
		$Xe_2@C_{60} \rightarrow C_{60}^{2-} + Xe_2^{2+}$	
$..(e_u)^4(a_{2u})^2(a_{2u})^0(e_u)^0$ ($^1A_{1g}$)	242.35 (*239.67*)	350.40 (*321.04*)	315.84 (*287.32*)
$..(e_u)^4(a_{2u})^1(a_{2u})^1(e_u)^0$ ($^3A_{1g}$)	237.17 (*234.84*)	353.79 (*324.40*)	319.76 (*290.83*)
$..(e_u)^4(e_u)^2(a_{2u})^0$ (^3E_u)	234.08 (*231.75*)	359.33 (*329.95*)	317.90 (*289.40*)

[a] Using BP86/TZVPP optimized geometries. [b] Values in *italics* are counterpoise corrected for the BSSE.

Table 10. Calculated values of the AIM analysis for Ng_2^{q+} ($q=0, 1, 2$) at BP86/TZVPP. Charge density at the bond critical point $\rho(r_b)$, Laplacian at the bond critical point $\nabla^2\rho(r_b)$, energy at the bond critical point $H(r_b)$.

Ng_2^{q+}	r(Ng–Ng)	$\rho(r_b)$ [e Å^{-3}]	$\nabla^2\rho(r_b)$ [e Å^{-5}]	$H(r_b)$ [Hartree Å^{-3}]
$[Kr_2]$	2.460	0.47	5.62	−0.07
$[Kr_2]^+$	2.460	0.50	3.84	−0.08
$[Kr_2]^{2+}$	2.460	0.53	1.64	−0.10
$[Xe_2]$	2.494	0.67	3.39	−0.28
$[Xe_2]^+$	2.494	0.71	1.70	−0.32
$[Xe_2]^{2+}$	2.494	0.75	−0.49	−0.35
Xe_2^+ opt	3.228	0.19	1.23	0.00
Xe_2^{2+} opt	2.736	0.50	0.29	−0.15

also given. Both sets of data will be compared with the AIM results of $Ng_2@C_{60}$ given in Table 4. The optimized bond lengths of Xe_2^{q+} are significantly longer than in the endohedral fullerene. We want to point out that even the theoretical value for Xe_2^{2+} (2.736 Å) is clearly bigger than for $Xe_2@C_{60}$ (2.494 Å). The AIM data for Kr_2^{q+} agree quite well with the data for $Kr_2@C_{60}$ when $q=0$. The AIM results for the Xe–Xe interactions in $Xe_2@C_{60}$ are intermediate between the values of Xe_2^+ and Xe_2^{2+}. The results of the AIM analysis and the calculated atomic partial charges support the suggestion that the interacting species in $Xe_2@C_{60}$ are Xe_2^{q+} and C_{60}^{q-}, where $1<q<2$.

To obtain more insight into the nature of the interactions between the confined $[Ng_2]$ species and the C_{60} cage we carried out EDA calculations of $Ng_2@C_{60}$ using $[Ng_2]$ and $[C_{60}]$ as fragments. The EDA study of $Xe_2@C_{60}$ was also carried out using Xe_2^{q+} and C_{60}^{q-} ($q=1, 2$) as interacting fragments. The results are shown in Table 11.

The EDA values indicate that the repulsive interactions between neutral $[Ng_2]$ and $[C_{60}]$ come from the Pauli repulsion ΔE_{Pauli}, which continuously increases from $He_2@C_{60}$ to $Xe_2@C_{60}$. Please note that the quasi-classical electrostatic interaction ΔE_{elstat} between the neutral fragments is always attractive. The calculated ΔE_{elstat} values rise from a weak attraction in $He_2@C_{60}$ ($\Delta E_{elstat}=-3.5$ kcal mol^{-1}) to a large value in $Xe_2@C_{60}$ ($\Delta E_{elstat}=-304.4$ kcal mol^{-1}). The latter value is even larger than the electrostatic attraction between $[Ng_2]^+$ and $[C_{60}]^-$ in $Xe_2@C_{60}$ ($\Delta E_{elstat}=-233.6$ kcal mol^{-1}), which is counterintuitive. An explanation for the large electrostatic attraction between neutral species has been given in recent theoretical studies of the chemical bond in nonpolar bonds.[53] The nucleus–electron attraction outbalances the nucleus–nucleus and electron–electron repulsions, which strongly increase when the nuclei become heavier. The quasi-classical electrostatic attraction in H_2 is so weak because the nuclear charges are small, which makes dihydrogen an atypical example of a covalent bond.[54] The electronic charge in $[Ng_2]^+$ is more compact than in $[Ng_2]$ and, therefore, it overlaps less with the carbon nuclei of the cage atoms, and is not compensated by the weaker shielding of the xenon nuclei. The two factors cancel in the electrostatic interactions between $[Ng_2]^{2+}$ and $[C_{60}]^{2-}$, which eventually yield stronger attractions in $Xe_2@$

Table 11. EDA results for D_{3d} $Ng_2@C_{60}$ at BP86/TZ2P. Energy values in kcal mol^{-1}.

Compound	$He_2@C_{60}$ $^1A_{1g}$	$Ne_2@C_{60}$ $^1A_{1g}$	$Ar_2@C_{60}$ $^1A_{1g}$	$Kr_2@C_{60}$ $^1A_{1g}$	$Xe_2@C_{60}$ $^1A_{1g}$	$Xe_2@C_{60}$ $^1A_{1g}$	$Xe_2@C_{60}$ $^1A_{1g}$	$Xe_2@C_{60}$ ^3E_u
Fragments	$[He_2]+[C_{60}]$	$[Ne_2]+[C_{60}]$	$[Ar_2]+[C_{60}]$	$[Kr_2]+[C_{60}]$	$[Xe_2]+[C_{60}]$	$[Xe_2^+]+[C_{60}]^-$	$[Xe_2^{2+}]+[C_{60}]^{2-}$	$[Xe_2^{2+}]+[C_{60}]^{2-}$
ΔE_{int}	7.9	22.3	87.2	135.7	205.5	90.1	−266.9	−256.9
ΔE_{pauli}	13.3	38.7	198.3	333.7	631.7	474.2	377.4	382.8
ΔE_{elstat}[a]	−3.5 (64.8)	−12.6 (76.6)	−84.0 (75.6)	−151.8 (76.6)	−304.4 (71.4)	−233.6 (60.8)	−351.7 (54.6)	−356.3 (55.7)
ΔE_{orb}[a]	−1.9 (35.2)	−3.8 (23.4)	−27.1 (24.4)	−46.3 (23.4)	−121.8 (28.6)	−150.5 (39.2)	−292.7 (45.4)	−283.4 (44.3)
$\Delta E_{orb}(a_{1g})$[b]	−0.8 (44.4)	−0.9 (22.7)	−4.4 (16.3)	−6.8 (14.7)	−9.0 (7.4)	−16.5 (11.0)	−25.1 (8.6)	−26.7 (9.4)
$\Delta E_{orb}(a_{2g})$[b]	0.0	<0.1 (0.3)	−0.1 (0.3)	−0.3 (0.5)	−0.9 (0.8)	−2.7 (1.8)	−5.5 (1.9)	−5.9 (2.1)
$\Delta E_{orb}(e_g)$[b]	−0.2 (9.0)	−0.9 (22.9)	−8.3 (30.7)	−14.1 (30.4)	−22.8 (18.7)	−44.2 (29.3)	−69.6 (23.8)	−74.1 (26.2)
$\Delta E_{orb}(a_{1u})$[b]	0.0	<0.1 (0.3)	−0.1 (0.4)	−0.3 (0.6)	−1.0 (0.8)	−3.2 (2.1)	−6.6 (2.2)	−7.0 (2.5)
$\Delta E_{orb}(a_{2u})$[b]	−0.7 (34.9)	−1.1 (27.9)	−4.8 (17.7)	−9.4 (20.2)	−63.1 (51.8)	−33.8 (22.4)	−106.6 (36.4)	−82.0 (28.9)
$\Delta E_{orb}(e_u)$[b]	−0.2 (11.6)	−1.0 (26.6)	−9.4 (34.6)	−15.5 (33.5)	−24.9 (20.5)	−50.2 (33.4)	−79.5 (27.1)	−87.8 (31.0)

[a] Values in parentheses give the percentage contribution to the total attractive interactions $\Delta E_{elstat}+\Delta E_{orb}$. [b] Values in parentheses give the percentage contribution to the total orbital interactions ΔE_{orb}.

C_{60} ($\Delta E_{elstat} = -351.7$ kcal mol^{-1} for the $^1A_{1g}$ state and $\Delta E_{elstat} = -356.3$ kcal mol^{-1} for the ^3E_u state).

The breakdown of the orbital term ΔE_{orb} into contributions from orbitals which have different symmetry reveals quantitatively the strength of the individual orbital interactions. The calculated data indicate that the strongest contributions in the heavier noble gas complexes come from the orbitals which have a_{2u}, e_g, and e_u symmetry. The a_{2u} contributions come from the σ^*orbitals of Ng_2, while the e_g and e_u contributions come from the bonding interactions of the occupied π^* and π orbitals, respectively. The attractive contribution of the σ orbitals of Ng_2, which have a_{1g} symmetry in the D_{3d} endohedral fullerenes, is clearly weaker.

Summary and Conclusion

The results of this work can be summarized as follows. The quantum chemical calculations predict that the equilibrium geometries of the endohedral fullerenes $Ng_2@C_{60}$ have D_{3d} symmetry when Ng = Ne, Ar, Kr, while the energy minimum structure of $Xe_2@C_{60}$ has D_{5d} symmetry. The precession movement of He_2 in $He_2@C_{60}$ has practically no barrier. The Ng–Ng distances in $Ng_2@C_{60}$ are much shorter than in free Ng_2. All compounds $Ng_2@C_{60}$ are thermodynamically unstable toward loss of the noble gas atoms. The heavier species $Ar_2@C_{60}$, $Kr_2@C_{60}$ and $Xe_2@C_{60}$ are high energy compounds which are at the BSSE corrected SCS-MP2/TZVPP level 96.7–305.5 kcal mol^{-1} less stable than free $C_{60} + 2Ng$. The AIM method shows that there is always an Ng–Ng bond path in $Ng_2@C_{60}$. There are six Ng–C bond paths in (D_{3d}) $Ar_2@C_{60}$, $Kr_2@C_{60}$, and $Xe_2@C_{60}$, while the lighter D_{3d} homologues $He_2@C_{60}$ and $Ne_2@C_{60}$ have only three Ng–C_2 paths. The calculated charge distribution and the orbital analysis clearly show that the bonding situation in $Xe_2@C_{60}$ significantly differs from those of the lighter homologues. The atomic partial charge of the [Xe_2] moiety is +1.06 while the charges of the lighter dimers [Ng_2] are close to zero. The a_{2u} HOMO of $Xe_2@C_{60}$ in the $^1A_{1g}$ state shows a large mixing of the highest lying occupied σ^* orbital of [Xe_2] and the orbitals of the C_{60} cage. There is only a small gap between the a_{2u} HOMO of $Xe_2@C_{60}$ and the e_u LUMO and the a_{2u} LUMO+1. The calculations show that there are several triplet states which are close in energy to each other and to the $^1A_{1g}$ state. The bonding analysis clearly shows that the interacting species in $Xe_2@C_{60}$ are Xe_2^{q+} and C_{60}^{q-}, where $1 < q < 2$. The calculated Xe–Xe distance in the endohedral fullerene (2.494 Å) is even shorter than the calculated bond length of free Xe_2^{2+} (2.746 Å).

It is illuminating to consider the results of the bonding analysis of $Ng_2@C_{60}$ in the light of the introductory comments about previous work. At the same time we want to address the question in the title of this work. The results give clear evidence that the Xe–Xe and the Xe_2–C_{60} interactions in $Xe_2@C_{60}$ should be considered as genuine chemical bonds. This can be explained with the change in the valence shell of Xe_2, which looses between 1 and 2 electrons to the C_{60} cage in $Xe_2@C_{60}$ due to the strong steric pressure of the fullerene. The Xe–Xe and Xe–C_{60} bonds can thus be explained in terms of traditional orbital and electrostatic interactions, which are common features of chemical bonds. At the other extreme of the endohedral fullerenes are $He_2@C_{60}$ and $Ne_2@C_{60}$, which have very weak Ng–Ng and Ng–C_{60} interactions. The encapsulated He_2, HeNe and Ne_2 species have been named "artifical molecules"[24] but is it justified to call them molecules when there is no genuine chemical bond? The IUPAC definition[1] may be called on in support of the classification of a chemical bond in $He_2@C_{60}$ and $Ne_2@C_{60}$, but this may not be satisfactory for adherents of a more traditional view of chemical bonding.[55] The chemical behavior of the latter species should not be very different from that of empty C_{60}, which becomes obvious by the finding that the ^{3}He NMR signal of $He_2@C_{60}$ is approximately the same as that of $He@C_{60}$.[22] From a chemical point of view, the two lightest endohedral fullerenes $He_2@C_{60}$ and $Ne_2@C_{60}$ are theoretically predicted to exhibit properties which are essentially the same as those of free C_{60}.

A different situation is given for the intermediate species $Ar_2@C_{60}$ and $Kr_2@C_{60}$. The optimized geometries (Table 1) show that the shortest C–C bond in free C_{60} (1.399 Å) becomes somewhat shorter in the two endohedral fullerenes (1.395 Å) while the longest bond of the free fullerene (1.454 Å) becomes considerably longer (1.477 Å and 1.489 Å). The changes of the C–C distances should influence the chemical reactivity of the C_{60} cage in addition reactions of $Ar_2@C_{60}$ and $Kr_2@C_{60}$. The chemical behavior of encapsulated [Ar_2] and [Kr_2] should also be quite different from that of free argon and krypton. This becomes obvious by comparing the calculated ε_{HOMO} values of [Ar_2] and [Kr_2] with free Ar and Kr, which are given in Table 6. The $\Delta\varepsilon_{HOMO}$ values at BP86/TZVPP of [Ar_2] (2.062 eV) and [Kr_2] (2.510 eV) clearly indicate that the valence electrons of the argon and krypton dimer are significantly better electron donors, which means that they are more reactive than free argon and krypton. The reactivity is further increased in the endohedral fullerenes $Ar_2@C_{60}$ and $Kr_2@C_{60}$ where the σ^* HOMO of [Ng_2] is even higher in energy (Table 6). In summary, the chemical reactivity of $Ar_2@C_{60}$ and $Kr_2@C_{60}$ is theoretically predicted to exhibit significant differences from free C_{60} and from free Ar and Kr. Thus, although the Ng–Ng and Ng–C interactions in the latter endohedral fullerenes may not be described in terms of traditional bonding models, they may be considered as genuine chemical bonds because the interatomic interactions of $Ar_2@C_{60}$ and $Kr_2@C_{60}$ yield independent molecules which possess a unique chemical reactivity. This view may be opposed by adherents of a more traditional view of chemical bonding, but most chemists will agree that the series of endohedral fullerenes $Ng_2@C_{60}$ exhibits a fascinating variety of interatomic interactions which question the classical view of a chemical bond.

Acknowledgements

We gratefully acknowledge stimulating discussions with and helpful suggestions by Prof. Einar Uggerud (Oslo). This work was supported by the Deutsche Forschungsgemeinschaft. Excellent service has been provided by the HRZ Marburg.

[1] a) *IUPAC Compendium of Chemical Terminology*, 2nd edition, **1997**. b) The more recent 2006 edition has the additional sentence: "The principle characteristic of a bond in a molecule is the existence of a region between the nuclei of constant potential contours that allows the potential energy to improve substantially by atomic contraction at the expense of only a small increase in kinetic energy." For the role of potential and kinetic energy in the chemical bond formation see reference [26].

[2] L. Pauling, *The Nature of the Chemical Bond*, 3d edition, Cornell University Press, Ithaca, New York, **1960**, p. 6.

[3] R. F. W. Bader, *J. Phys. Chem. A* **1998**, *102*, 7314.

[4] C. F. Matta, J. Hernández-Trujillo, T.-H. Tang, R. F. W. Bader, *Chem. Eur. J.* **2003**, *9*, 1940.

[5] A. Haaland, D. J. Shorokhov, N. V. Tverdova, *Chem. Eur. J.* **2004**, *10*, 4416.

[6] R. F. W. Bader, D.-C. Fang, *J. Chem. Theory Comput.* **2005**, *1*, 403.

[7] J. Poater, M. Solà, F. M. Bickelhaupt, *Chem. Eur. J.* **2006**, *12*, 2889.

[8] R. F. W. Bader, *Chem. Eur. J.* **2006**, *12*, 2896.

[9] J. Poater, M. Solà, F. M. Bickelhaupt, *Chem. Eur. J.* **2006**, *12*, 2902.

[10] A. Almenningen, O. Bastiansen, L. Fernholt, B. N. Cyvin, S. J. Cyvin, S. Samdal, *J. Mol. Struct.* **1985**, *128*, 59.

[11] A unicorn is a mystical creature whose appearance is known to everybody although nobody has ever seen one. For a discussion of unicorns in chemistry, see: G. Frenking, A. Krapp, *J. Comput. Chem.* **2007**, *28*, 15.

[12] For a comprehensive discussion of the present understanding of chemical bonding models see the 37 articles which appeared in the special edition entitled "90 years of chemical bonding": *J. Comput. Chem.* **2007**, *28*.

[13] M. Otto, S. D. Lotz, G. Frenking, *Inorg. Chem.* **1992**, *31*, 3647.

[14] A model for the bonding interactions in metastable dications has been suggested in: a) G. Frenking, W. Koch, D. Cremer, J. Gauss, J. F. Liebman, *J. Phys. Chem.* **1989**, *93*, 3397. The nature of the bonding in dications has been discussed in: b) J. Senekowitch, S. V. O'Neil, W. Meyer, *Theor. Chim. Acta* **1992**, *84*, 85. An overview about dications is given in: c) V. G. Nenajdenko, N. E. Shevchenko, E. S. Balenkova, I. V. Alabugin, *Chem. Rev.* **2003**, *103*, 229; d) D. Schröder, H. Schwarz, J. *Phys. Chem. A* **1999**, *103*, 7385; e) P. M. W. Gill, L. Radom, *J. Am. Chem. Soc.* **1989**, *111*, 4613.

[15] L. Pauling, *J. Chem. Phys.* **1933**, *1*, 58.

[16] A. Belkacem, E. P. Kanter, R. E. Mitchell, Z. Vager, B. J. Zabransky, *Phys. Rev. Lett.* **1989**, *63*, 2555.

[17] a) M. Kolbuszewski, J.-P. Gu, *J. Chem. Phys.* **1995**, *103*, 7649; b) J. Ackermann, H. Hogreve, *J. Phys. B* **1992**, *25*, 4069.

[18] a) W. Koch, G. Frenking, J. Gauss, D. Cremer, J. R. Collins, *J. Am. Chem. Soc.* **1989**, *111*, 4613; b) G. Frenking, D. Cremer, *Structure and Bonding, Vol. 73*, Springer, Heidelberg, **1990,** p. 17–95.

[19] R. J. Cross, M. Saunders, H. Prinzbach, *Org. Lett.* **1999**, *1*, 1479.

[20] H. A. Jimenez-Vazquez, J. Tamariz, R. J. Cross, *J. Phys. Chem. A* **2001**, *105*, 1315.

[21] D. Moran, F. Stahl, E. D. Jemmis, H. F. Schaefer III, P. v. R. Schleyer, *J. Phys. Chem. A* **2002**, *106*, 5144.

[22] T. Sternfeld, R. E. Hoffman, M. Saunders, R. J. Cross, M. S. Syamala, M. Rabinovitz, *J. Am. Chem. Soc.* **2002**, *124*, 8786.

[23] a) M. Straka, J. Vaara, *J. Phys. Chem. A* **2006**, *110*, 12338; b) R. B. Darzynkiewicz, G. E. Scuseria, *J. Phys. Chem. A* **1997**, *101*, 7141.

[24] a) J. Laskin, T. Peres, C. Lifshitz, M. Saunders, R. J. Cross, A. Khong, *Chem. Phys. Lett.* **1998**, *285*, 7; b) T. Peres, B. Cao, W. Cui, A. Khong, R. J. Cross, Jr., M. Saunders, C. Lifshitz, *Int. J. Mass Spectrom.* **2001**, *210/211*, 241.

[25] M. Saunders, H. A. Jimenez-Vazquez, R. J. Cross, S. Mroczkowski, M. L. Gross, D. E. Giblin, R. J. Poreda, *J. Am. Chem. Soc.* **1994**, *116*, 2193.

[26] T. Bitter, K. Ruedenberg, W. H. E. Schwarz, *J. Comput. Chem.* **2007**, *28*, 411.

[27] a) A. D. Becke, *Phys. Rev. A* **1988**, *38*, 3098; b) J. P. Perdew, *Phys. Rev. B* **1986**, *33*, 8822.

[28] F. Weigend, R. Ahlrichs, *Theor. Chem. Acc.* **1997**, *97*, 331.

[29] F. Weigend, R. Ahlrichs, *Phys. Chem. Chem. Phys.* **2005**, *7*, 3297.

[30] K. A. Peterson, D. Figgen, E. Goll, H. Stoll, M. Dolg, *J. Chem. Phys.* **2003**, *119*, 11113.

[31] a) C. Møller, M. S. Plesset *Phys. Rev.* **1934**, *46*, 618; b) J. S. Binkley, J. A. Pople, *Int. J. Quantum Chem.* **1975**, *9S*, 229.

[32] S. Grimme, *J. Chem. Phys.* **2003**, *118*, 9095.

[33] S. Grimme, *J. Phys. Chem.* A **2005**, *109*, 3067.

[34] S. F. Boys, F. Bernardi, *Mol. Phys.* **1970**, ***19***, 558.

[35] R. Ahlrichs, M. Baer, M. Haeser, H. Horn, C. Koelmel, *Chem. Phys. Lett.* **1989**, *162*, 165.

[36] R. Ahlrichs, K. May, *Phys. Chem. Chem. Phys.* **2000**, *2*. 943.

[37] A. E. Reed, L. A. Curtiss, F. Weinhold, *Chem. Rev.* **1988**, *88*, 899.

[38] R. F. W. Bader, *Atoms in Molecules. A Quantum Theory*, Oxford University Press, Oxford, **1990**.

[39] AIMPAC Program Package, R. F. W. Bader research group, McMaster University, Hamilton, Canada.

[40] a) T. Ziegler, A. Rauk, *Theor. Chim. Acta* **1977**, *46*, 1; b) K. Morokuma, *J. Chem. Phys.* **1971**, *55*, 1236.

[41] J. G. Snijders, E. J. Baerends, P. Vernooijs, *At. Nucl. Data Tables* **1982**, *26*, 483.

[42] a) F. M. Bickelhaupt, E. J. Baerends, *Rev. Comput. Chem.* **2000**, *15*, 1; b) G. te Velde, F. M. Bickelhaupt, E. J. Baerends, S. J. A. van Gisbergen, C. Fonseca Guerra, J. G. Snijders, T. Ziegler, *J. Comput. Chem.* **2001**, *22*, 931.

[43] For reviews about the application of the EDA see reference [42a] and the following: a) M. Lein, G. Frenking in *Theory and Applications of Computational Chemistry: The First 40 Years*, (Eds.: C. E. Dykstra, G. Frenking, K. S. Kim, G. E. Scuseria), Elsevier, Amsterdam, **2005,** p. 367; b) G. Frenking, K. Wichmann, N. Fröhlich, C. Loschen, M. Lein, J. Frunzke, V. M. Rayón, *Coord. Chem. Rev.* **2003**, *238–239*, 55.

[44] The calculated values for He_2, Ne_2, and Ar_2 have been taken from: T. J. Giese, D. M. York, *Int. J. Quantum Chem.* **2004**, *98*, 388. The values for Kr_2 and Xe_2 have been taken from: P. Slavicek, R. Kalus, P. Paska, I. Odvarkova, P. Hobza, A. Malijevsky, *J. Chem. Phys.* **2003**, *119*, 2102.

[45] J. F. Ogilvie, F. Y. Wang, *J. Mol. Struct.* **1992**, *273*, 277.

[46] T. Drews, K. Seppelt, *Angew. Chem.* **1997**, *109*, 264; *Angew. Chem. Int. Ed. Engl.* **1997**, *36*, 273.

[47] M. Bühl, S. Patchkovski, W. Thiel, *Chem. Phys. Lett.* **1997**, *275*, 14.

[48] The system $Ng@C_{60}$ (Ng = He–Xe) has also been studied at the MP2/DZP level in reference [23b]. The authors report in the latter work that the dissociation reaction $Ng@C_{60} \rightarrow C_{60}+Ng$ is exothermic which means that the endohedral fullerenes should be thermodynamically unstable. The results have been corrected: R. B. Darzynkiewicz, G. E. Scuseria, *J. Phys. Chem. A* **1998**, *102*, 3458.

[49] It is important to point out that steric repulsion is not caused by electrostatic interactions but solely by the Pauli repulsion which prohibits the overlap of occupied orbitals for electrons which possess the same spin. For a detailed discussion see reference 53.

[50] We use the D_{3d} structure for $Xe_2@C_{60}$ to compare it with the same isomeric form of the other endohedral fullerenes. The differences between the electronic structures of the D_{3d} form and the D_{5d} form of $Xe_2@C_{60}$ are negligible.

[51] D. Cremer, E. Kraka, *Angew. Chem.* **1984**, *96*, 612; *Angew. Chem. Int. Ed. Engl.* **1984**, *23*, 62.

[52] There are actually two triplet states which can be formed when two unpaired electrons occupy the two components of the vacant e_u orbital and the resulting triplet state may have $^3A_{1u}$ or ^3E_u symmetry. The two states should be very close in energy.

[53] a) A. Krapp, F. M. Bickelhaupt, G. Frenking, *Chem. Eur. J.* **2006**, *12*, 9196; b) A. Kovács, C. Esterhuysen, G. Frenking, *Chem. Eur. J.* **2005**, *11*, 1813; c) C. Esterhuysen, G. Frenking, *Theor. Chem. Acc.* **2004**, *111*, 381. Erratum: **2005**, 113, 294.
[54] a) M. A. Spackman, E. N. Maslen, *J. Phys. Chem.* **1986**, *90*, 2020; b) F. L. Hirshfeld, S. Rzotkiewicz, *Mol. Phys.* **1974**, *27*, 1319.
[55] One referee rightfully pointed out that the IUPAC definition which was suggested by Pauling was not designed for endohedral fullerenes. The results of this work clearly show that the objects of modern chemistry may not easily be defined in terms of classical models of chemistry. This holds, for example, for nanochemistry, where the interactions between the encapsulated species and the tubes are difficult to describe in terms of local bonds.

Received: March 26, 2007
Published online: July 18, 2007

